Biosynthesis of silver and gold nanoparticles by novel sundried *Cinnamomum camphora* leaf

2007 Nanotechnology 18 105104

(http://iopscience.iop.org/0957-4484/18/10/105104)

IOP PUBLISHING NANOTECHNOLOGY
Nanotechnology **18** (2007) 105104 (11pp) doi:10.1088/0957-4484/18/10/105104

Biosynthesis of silver and gold nanoparticles by novel sundried *Cinnamomum camphora* leaf

Jiale Huang[1,2], Qingbiao Li[1,2,3], Daohua Sun[1], Yinghua Lu[1,2], Yuanbo Su[1,2], Xin Yang[1,2], Huixuan Wang[1,2], Yuanpeng Wang[1], Wenyao Shao[1], Ning He[1], Jinqing Hong[1] and Cuixue Chen[1]

[1] Department of Chemical and Biochemical Engineering, College of Chemistry and Chemical Engineering, Xiamen University, Xiamen 361005, People's Republic of China
[2] Key Lab for Chemical Biology of Fujian Province, Xiamen University, Xiamen 361005, People's Republic of China

E-mail: kelqb@xmu.edu.cn

Received 27 October 2006, in final form 16 January 2007
Published 6 February 2007
Online at stacks.iop.org/Nano/18/105104

Abstract
The synthesis of nanocrystals is in the limelight in modern nanotechnology. Biosynthesis of nanoparticles by plant extracts is currently under exploitation. Not only could silver nanoparticles ranging from 55 to 80 nm in size be fabricated, but also triangular or spherical shaped gold nanoparticles could be easily modulated by reacting the novel sundried biomass of *Cinnamomum camphora* leaf with aqueous silver or gold precursors at ambient temperature. The marked difference of shape control between gold and silver nanoparticles was attributed to the comparative advantage of protective biomolecules and reductive biomolecules. The polyol components and the water-soluble heterocyclic components were mainly responsible for the reduction of silver ions or chloroaurate ions and the stabilization of the nanoparticles, respectively. The sundried leaf in this work was very suitable for simple synthesis of nanoparticles.

S Supplementary data are available from stacks.iop.org/Nano/18/105104

(Some figures in this article are in colour only in the electronic version)

1. Introduction

Proliferation of nanotechnology has opened up novel fundamental and applied frontiers in materials science and engineering, such as quantum dots [1], surface-enhanced Raman scattering (SERS) [2] and nanobiotechnology [3]. Among them, nanobiotechnology is the multidisciplinary integration of biotechnology, nanotechnology, chemical processing, physical methodology and systems engineering into biochips, molecular motors, nanocrystals and nanobiomaterials [3]. In the last decade, biosynthesis of nanoparticles as an emerging highlight of the intersection of nanotechnology and biotechnology has received increasing attention due to a growing need to develop environmentally benign technologies in material syntheses. The significance of such a synthetic protocol has been well demonstrated [4, 5]. For instance, a great deal of effort has been put into the biosynthesis of inorganic materials, especially metal nanoparticles, using microorganisms [5] and plants [6]. Both live microorganisms and dead microorganisms are gaining importance by virtue of their facile assembly of nanoparticles. Prokaryotic bacteria have primarily attracted the most attention in the area of biosynthesis of metal nanoparticles [5]. A significant demonstration of biosynthesis by prokaryotic bacteria was reported by Klaus *et al*, who described the phenomenon of biosynthesis of silver-based single crystals at the cell poles of propagating *Pseudomonas stutzeri* AG259 [7]. Fu *et al* reported biosorption and bioreduction of silver ions by dried *Lactobacillus sp*. A09 [8]. Otherwise, Nair *et al* showed the formation of submicron crystallites of Ag, Au and Ag–

[3] Author to whom any correspondence should be addressed.

Au alloy assisted by live *Lactobacillus* strains and their SERS applications [9]. It was very interesting that Macaskie *et al* had showed the rapid reduction of Pd(II) to Pd(0) by using *Desulfovibrio desulfuricans* NCIMB 9307 at the expense of formate or H_2 as electron donors [10]. Our group explored biosorption and bioreduction of diamine silver complex by dried *Corynebacterium sp.* SH09 and *Aeromonas sp.* SH10 isolated from a gold mine [11, 12]. Importantly, Sastry *et al* had opened an avenue to the synthesis of metal nanoparticles by eukaryotic organisms [13, 14]. Later, they continued to accomplish some excellent work based on fungi, especially extracellular synthesis of Ag or Au nanoparticles [15–18]. They demonstrated that the shift from bacteria to fungi as a means of developing natural 'nano-factories' has the added advantage that processing and handling of the biomass would be much simpler [16].

The biosynthetic method employing plant extracts has received some attention as a simple and viable alternative to chemical procedures and physical methods synthesizing metal nanoparticles only in recent years. Jose-Yacaman *et al* firstly reported the formation of gold and silver nanoparticles by living plants [19, 20]. Sastry *et al* aforementioned attained the biosynthesis of metal nanoparticles by plant leaf extracts and their potential applications [21–29]. They studied bioreduction of chloroaurate ions or silver ions by a broth of geranium leaf [21, 22] or Neem leaf [23]. Further, they had explored the formation mechanism of gold nanotriangles by lemongrass extracts. The nanotriangles seemed to grow by a process involving rapid reduction, assembly and room-temperature sintering of 'liquid-like' spherical gold nanoparticles [24]. Then they had also synthesized gold nanotriangles using Tamarind leaf extract and studied their potential application in vapour sensing [26]. Very recently, they have demonstrated synthesis of gold nanotriangles and silver nanoparticles using *Aloe vera* plant extracts [29]. It was explained that only biomolecules of MWs less than 3 kDa caused reduction of chloroaurate ions, leading to the formation of gold nanotriangles. Nevertheless, the bioreduction of silver ions proceeded merely in the presence of ammonia. Most of the above research on the synthesis of silver or gold nanoparticles utilizing plant extracts employed broths resulting from boiling fresh plant leaves [21–29]. Here, novel sundried *C. camphora* leaf, previously unexploited for bioreduction and different from such boiling procedures, was used to synthesize silver and gold nanoparticles in aqueous solutions at ambient conditions, without any additive protecting nanoparticles from aggregating, template shaping nanoparticles or accelerants like ammonia. Comparative experiments were carried out to investigate the effect of the biomass dosage on bioreduction and uniformity of the nanoparticles. The pronounced difference of shape control between gold and silver nanoparticles was also discussed. To have a good insight into the bioreduction, FTIR analyses of the dried biomass and the dried nanoparticles were conducted. The approach appears to be a cost-efficient alternative to conventional methods of assembling silver and gold nanoparticles so that it would be suitable for developing a biological process for large scale production. It has been reported very recently by our group that some pharmacological anticancer components could be extracted from *C. camphora* leaf [30].

2. Experimental details

2.1. Preparation of dried biomass

*Cinnamomum camphora*trees were cultivated by Xiamen Peony Perfume&Chemicals Industry Co. Ltd, China. The freshly harvested *C. camphora* leaves were exposed to the sun until they were completely dried. The biomass used for the reduction was prepared by crushing the dried leaves and then screening the leaf powder by a 20 mesh sieve.

2.2. Synthesis for silver and gold nanoparticles

Two chemicals, silver nitrate ($AgNO_3$) and chloroauric acid ($HAuCl_4$), were purchased from Sinopharm Chemical Reagent Co. Ltd, China and were used as received. In a typical synthesis for silver and gold nanoparticles using dried powder of *C. camphora* leaf, the carefully weighted biomass was added to 50 ml of 1 mM aqueous $AgNO_3$ and $HAuCl_4$ solution, respectively, in conical flasks of 100 ml content at room temperature. The flasks were thereafter shaken at a rotation rate of 150 rpm in the dark at 30 °C.

2.3. UV–vis spectra analysis

The bioreduction of Ag^+ or $AuCl_4^-$ in aqueous solution was monitored by periodic sampling of aliquots (0.2 ml) of the suspension, then diluting the samples with 2 ml deionized water and subsequently measuring UV–vis spectra of the resulting diluents. UV–vis spectroscopy analyses of silver or gold nanoparticles produced were carried out as a function of bioreduction time at room temperature on UNICAM UV-300 spectrophotometers (Thermo Spectronic) at a resolution of 1 nm.

2.4. XRD measurement

After bioreduction, the residual solutions consisting of hydrosols and residual biomass were dried at 60 °C and the dried mixture was collected for the determination of the formation of Ag or Au by an X'Pert Pro x-ray diffractometer (PANalytical BV, The Netherlands) operated at a voltage of 40 kV and a current of 30 mA with Cu Kα radiation.

2.5. TEM observation of silver and gold nanoparticles, and SEM and AFM observation of gold nanotriangles

The biomass after reaction spontaneously precipitated at the bottom of the conical flasks in 1 h. After the precipitation, the suspension above the precipitate was sampled for TEM observation. TEM samples of the aqueous suspension of silver or gold nanoparticles were prepared by placing a drop of the suspension on carbon-coated copper grids and allowing water to evaporate. TEM observations were performed on a H-600 electron microscope (Hitachi, Japan) operated at an accelerating voltage of 120 kV. Size distribution of the resulting nanoparticles was estimated on the basis of TEM micrographs with the assistance of SigmaScan Pro software (SPSS Inc, Version 4.01.003). High-resolution TEM images were obtained and energy dispersive x-ray (EDX) analyses were performed on a Tecnai F30 microscope. SEM samples of the aqueous suspension of gold nanotriangles were fabricated

by dropping the suspension onto clean electric glass (Xiamen Ito Photoelectricity Industry Co. Ltd, China) and allowing water to completely evaporate. SEM observations were carried out on a LEO-1530 electron microscope (LEO, Germany). The suspension of gold nanotriangles was cast onto a graphite substrate and they were measured by AFM in the contact mode on a multimode scanning probe microscope (Digital Instrument, USA) with a Nanoscope IIIa controller.

2.6. FTIR analysis of dried biomass before and after bioreduction

After bioreduction, the biomass residue was obtained by centrifuging the residual solution at 4800 rpm for 10 min. Then the biomass residue was completely dried at 60 °C. The dried biomass before bioreduction and the residue of *C. camphora* leaf after bioreduction were analysed by FTIR Nicolet Avatar 660 (Nicolet, USA).

2.7. FTIR analysis of silver and gold nanoparticles

To remove any free biomass residue or compound that is not the capping ligand of the nanoparticles, the residual solution of 10 ml after reaction was centrifuged at 4800 rpm for 10 min and the resulting suspension was redispersed in 20 ml sterile distilled water. The centrifuging and redispersing process was repeated three times. Thereafter, the purified suspension was completely dried at 60 °C. Finally, the dried nanoparticles were analysed by FTIR Nicolet Avatar 660 (Nicolet, USA).

3. Results and discussion

3.1. Biosynthesis of silver nanoparticles by C. camphora leaf

It is generally recognized that UV–vis spectroscopy could be used to examine size- and shape-controlled nanoparticles in aqueous suspensions [31]. Given the constant aqueous $AgNO_3$ (50 ml, 1 mM), comparative experiments were carried out to investigate the effect of different amounts of the dried biomass on bioreduction and uniformity of target products. The amount of the dried biomass was found to play a critical role in size dispersity of silver nanoparticles. Figure 1 shows the absorption spectra of silver nanoparticles produced by different amounts of the dried biomass, revealing the production of silver nanoparticles within 1 h after silver ions came in contact with the biomass. After addition of the biomass to the solution of silver nitrate, the solution changed from colourless to pale green in about 1 h, the final colour deepening with the increase of the dried biomass. The evolution of the absorbance spectra emanating from silver nanoparticles over time manifests increasingly sharp absorbance with increasing time of reaction at around 440 nm. Only absorbance peaks at about 440 nm may be identified in figure 1(a), obtained by gently reducing $AgNO_3$ with 0.1 g biomass. However, distinguished from figure 1(a), weak absorbance peaks at about 360 nm may be perceived in figure 1(b), acquired by mild reduction of silver ions with 0.5 g biomass. The weak peaks become more apparent in figure 1(c), prepared by rapidly reducing $AgNO_3$ with 1.0 g biomass, than in figure 1(b). The difference may be explained by representative TEM images shown in figure 2 recorded at different magnifications of

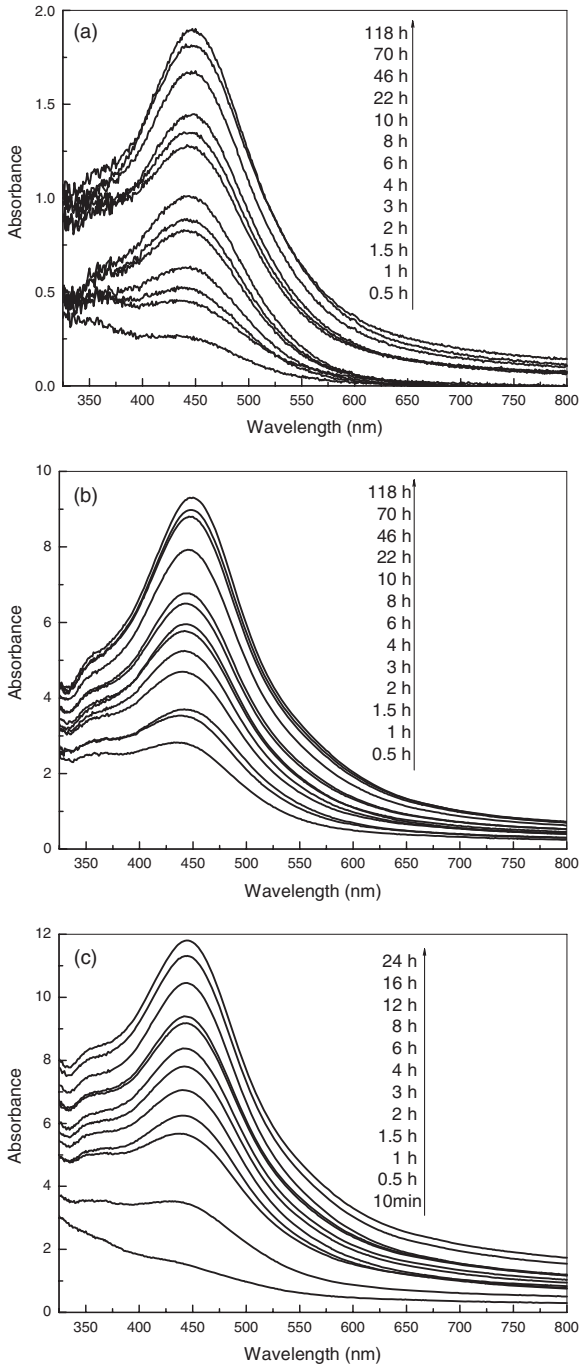

Figure 1. Absorption spectra of silver nanoparticles after bioreduction by dried powder of *C. camphora* leaf at 30 °C. The biomass, (a) 0.1 g, (b) 0.5 g and (c) 1.0 g, was exposed to 50 ml, 1 mM aqueous solution of $AgNO_3$.

particles resulting from the reaction of silver ions and different amounts of the dried biomass. Figure 2(a) displays the TEM image of typical nanoparticles, produced by 0.1 g biomass, showing that the as-formed nanoparticles were quantitatively sparse. It could be easily figured out from figure 1 that insufficiency of the reductive biomolecules for reduction of silver ions was responsible for the formation of the few particles, as the maximum absorbance in figure 1(a) is much lower than that in figures 1(b) and (c). Figures 2(b) and (c)

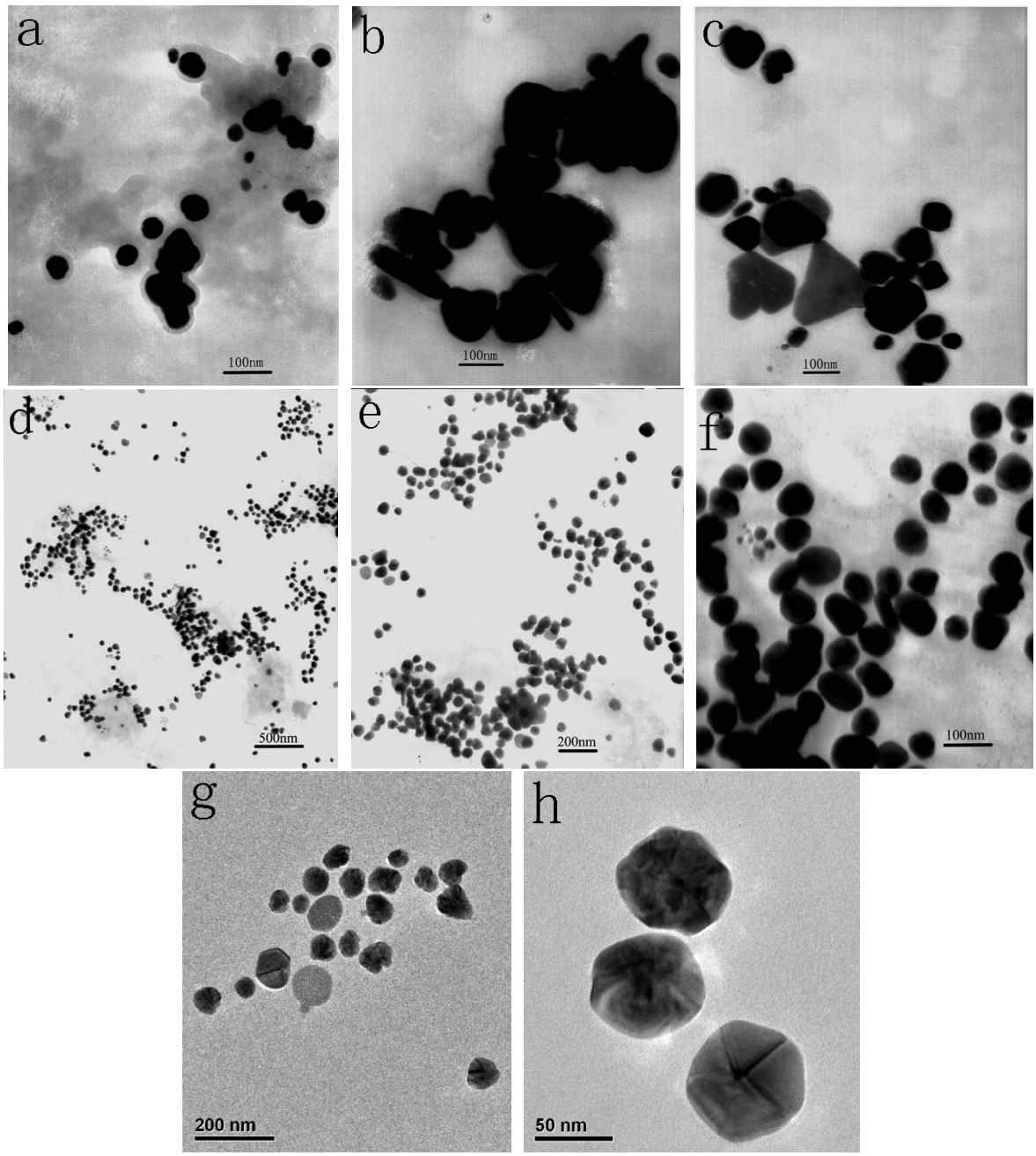

Figure 2. Transmission electron micrographs of silver nanoparticles after bioreduction. The biomass, (a) 0.1 g, (b) and (c) 1.0 g, and (d)–(h) 0.5 g, was exposed to 50 ml, 1 mM aqueous solution of $AgNO_3$ at 30 °C. Scale bars: (a)–(c) 100 nm; (d) 500 nm; (e) 200 nm; (f) 100 nm; (g) 200 nm; (h) 50 nm.

exhibit the TEM images of typical nanoparticles, which were obtained by 1.0 g biomass. The resulting nanoparticles, however, were polydisperse. Some anisotropic nanostructures, such as nanotriangles or nanoparticles with irregular contours, could be observed in figures 2(b) and (c). As a result, they posed another detectable absorbance at around 360 nm, besides the absorbance at about 440 nm as seen in figure 1(c). However, the overall morphology of the sample produced by mild reduction of silver ions with 0.5 g biomass is shown in figure 2(d), which indicates that the sample is composed of a large quantity of largely uniform nanoparticles. According to size distribution of the silver nanoparticles shown in figure 3, the nanoparticles, mostly ranging from 55 to 80 nm in size, possess a narrow size distribution. Figures 2(e) and (f) show the morphology of the sample with higher magnification and the average diameter of these nanoparticles was evaluated to be about 64.8 nm. The size distribution could be further verified by high-resolution TEM images of the nanoparticles in the same suspension, as depicted in figures 2(g) and (h). A few ellipsoidal nanoparticles observed in figure 2(f) bring about another weak absorbance at around 360 nm, besides those at about 440 nm as seen in figure 1(b). Lots of

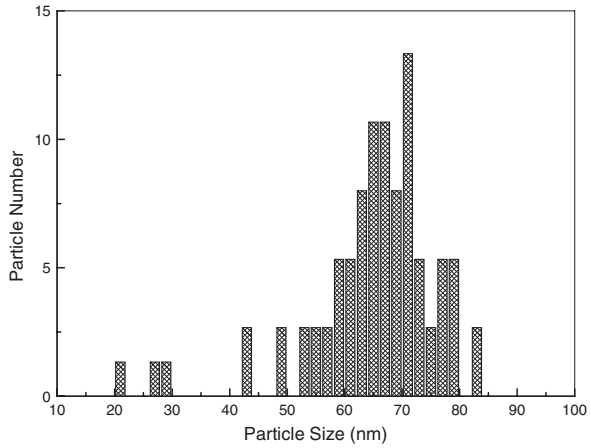

Figure 3. A histogram of size distribution of silver nanoparticles synthesized by the experiment using 0.5 g biomass. The average particle size is 64.8 nm.

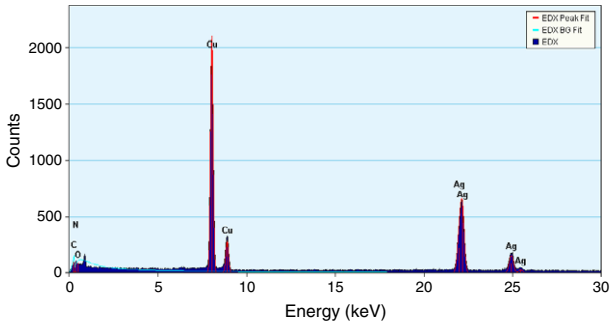

Figure 4. Energy dispersive x-ray spectrum of silver nanoparticles resulting from the experiment using 0.5 g biomass. The different x-ray emission peaks are labelled.

nanoparticles in figures 2(d) and (e) tended to congregate in solution into clusters, unlike quasi-linear superstructures illustrated by Sastry *et al* [22]. It could be concluded that silver nanoparticles from rapid bioreduction were polydisperse while those from mild reduction were nearly quasi-spherical. In general, the particle size in figures 2(d) and (e) was larger than that reported by Sastry *et al* using leaf broth [22, 25, 29]. The particles were verified to contain a great deal of Ag using EDX analysis in figure 4 and confirmed as elemental Ag(0) using XRD as shown in figure 5. Pattern 1 in figure 5 shows the typical XRD pattern of the sundried leaf before bioreduction. Pattern 2, pattern 3 and pattern 4 are XRD results of silver nanoparticles and the biomass residue after completion of the reaction. In contrast to pattern 1, a couple of Bragg reflections are distinctly exhibited in pattern 2, pattern 3 and pattern 4, which may be indexed on the basis of the face-centred cubic structure of silver. The XRD patterns thus clearly show that the silver nanoparticles are essentially crystalline. Additionally, the diffractions at around $2\theta = 22°$ resulting from the biomass or the biomass residue are also notable.

3.2. Biosynthesis of gold nanoparticles by C. camphora leaf

Likewise, given the constant aqueous $HAuCl_4$ (50 ml, 1 mM), comparative experiments were performed to investigate the

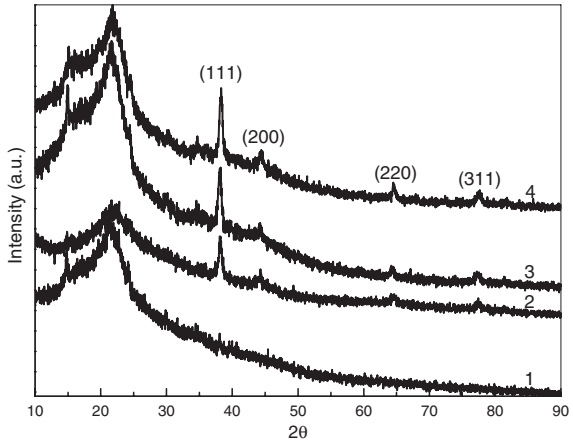

Figure 5. X-ray diffraction patterns of the as-prepared nanoparticles. Labelled peaks correspond to the characteristic diffraction peaks of elemental Ag(0). Pattern 1 was obtained by XRD analysis of the sundried leaf. Patterns 2, 3 and 4 were derived from XRD analysis of the dried mixtures after reaction of 0.1, 0.5 and 1.0 g biomass with 50 ml, 1 mM aqueous solution of $AgNO_3$, respectively.

effect of different dosages of the dried biomass on bioreduction and the properties of products. UV–vis spectra that were recorded at different intervals for the reaction of 0.1 g biomass with the aqueous $HAuCl_4$ show the appearance of a surface plasmon resonance (SPR) band at about 570 nm after 2 min of reaction, which increased in intensity with time, accompanied by the advent of a broad absorbance around 1000 nm after 60 min of reaction, as shown in figure 6(a). Nevertheless, by subjecting 0.5 g biomass to the same chloroauric acid, UV–vis spectra, from curve 1 to curve 4 recorded in figure 6(b), show the appearance of a SPR band at about 570 nm after 2 min of reaction, which shifts to about 530 nm in increasing intensity with time, while the longer absorbance is not present. Curve 5 recorded at 60 min of reaction by exposing the biomass of 1.0 g dosage to the aqueous $HAuCl_4$ still showed single absorbance at about 520 nm. The prominent difference of the spectra may be supported by representative TEM images shown in figure 7 recorded at different magnifications of gold particles resulting from the reduction of chloroaurate ions by different amounts of the dried biomass. Gold nanotriangles with a flat, platelike morphology, as described by Sastry *et al* [24], could lead to the longer absorbance in the near-infrared (NIR) region [24]. We observed that there were plenty of well-defined nanotriangles together with some quasi-spherical nanoparticles in a final sample shown in figures 7(a)–(c) as well as in the SEM image (see supplementary online material, figure S1 available at stacks.iop.org/Nano/18/105104). The coexistence of triangular and spherical particles in the observed hydrosol results in the two absorbance at around 570 and 1000 nm in figure 6(a), respectively. Figure 7(d) displays an individual nanotriangle tilting against carbon-coated copper grids. The thickness of typical nanotriangles could be measured to be about 7.0 nm by AFM (see supplementary online material, figure S2 available at stacks.iop.org/Nano/18/105104), comparable to the previous results [24, 26, 27, 29]. All the nanotriangles under low-resolution TEM observation are ostensibly flat. In essence, a high-resolution TEM image, i.e. figure 7(e), reveals a bumpy surface of another individual nanotriangle with nonuniform

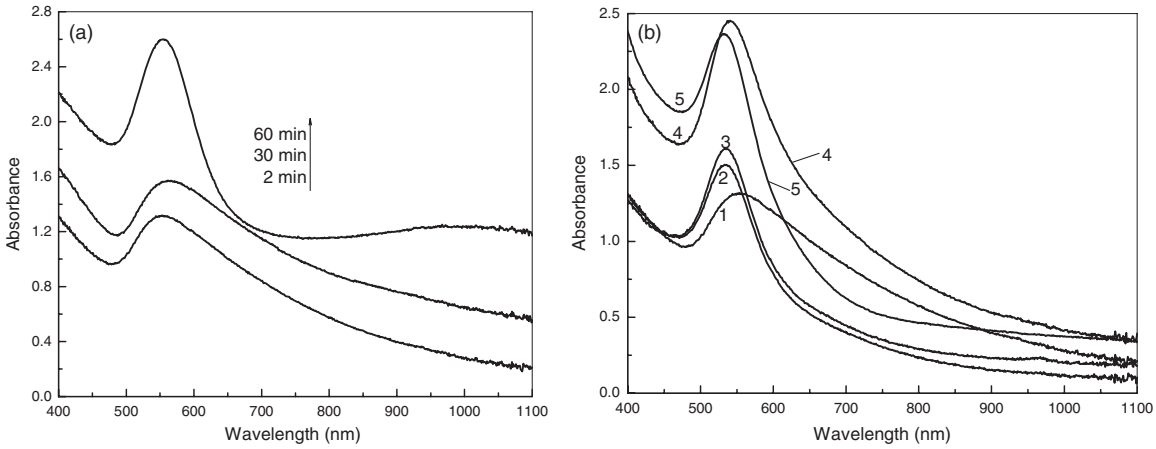

Figure 6. Absorption spectra of gold nanoparticles after bioreduction by dried powder of *C. camphora* leaf at 30 °C. (a) The biomass of 0.1 g dosage was exposed to 50 ml, 1 mM aqueous solution of $HAuCl_4$. (b) Curve 1–4 arise by exposing the biomass of 0.5 g dosage to 50 ml, 1 mM aqueous solution of $HAuCl_4$. The reaction time of curves 1, 2, 3 and 4 corresponds to 2, 20, 60 and 90 min, respectively. Curve 5 is recorded at 60 min of reaction by exposing the biomass of 1.0 g dosage to 50 ml, 1 mM aqueous solution of $HAuCl_4$.

'liquid-like' colour [24]. However, by switching the amount of the dried biomass from 0.1 to 0.5 g subjected to the same chloroauric acid, the particles shifted from nanotriangles to spherical particles shown in figure 7(f). It is interesting that spherical nanoparticles remain the dominant product in figure 7(g) when the dosage of dried biomass was increased to 1.0 g. In the light of edge length distribution, as depicted in figure 8(a), of the nanotriangles in figures 7(a)–(c), the average edge length was ascertained to be about 80 nm, smaller than previous studies [24, 26–29]. The spherical nanoparticles by the biomass of 0.5 g dosage in figure 7(f) have a size range from 10 to 40 nm and the average particle size was calculated to be around 23.4 nm, as shown in figure 8(b). Although those by the biomass of 1.0 g dosage in figure 7(g) also have the same size range, as shown in figure 8(c), they fall within the narrow size range from 15 to 25 nm with very high frequency and possess a narrower size distribution and smaller average diameter, about 21.5 nm, than that by 0.5 g biomass. The variation of the two average particle sizes is in good agreement with the shift from 530 nm absorbance of curve 4 to 520 nm absorbance of curve 5 in figure 6(b). The frequency and width of the surface plasmon absorption depends on the size and shape of the metal nanoparticles as well as on the dielectric constant of the metal itself and the surrounding medium [32]. Supposing the same particle shape, medium dielectric constant and temperature, the mean diameter of gold nanoparticles strongly influences the SPR band in aqueous solution [33]. The reduction of mean diameter of the nanoparticles could induce a blue shift of the SPR band. The blue shift from 530 to 520 nm with the biomass dosage increasing from 0.5 to 1.0 g is attributed to the overall diminution of gold particle size. The triangular particles were verified to contain a great deal of gold using energy dispersive x-ray spectrometry, as manifested in figure 9. Figure 10 shows typical x-ray diffraction patterns of the as-prepared sample and the sundried leaf before bioreduction, respectively. All the reflection peaks in pattern 2, pattern 3 and pattern 4 can be indexed to face-centred cubic gold. The XRD patterns show that the gold nanoparticles are also crystalline in nature.

Apparently, the reduction of chloroaurate ions was much more rapid than that of silver ions. On adding the dried biomass to aqueous chloroauric acid, the colour of the shaken solution changed from pale yellow to vivid ruby red, indicating formation of gold nanoparticles almost at the beginning of the reaction. Merely the absorbance peaks at ca. 570 nm were detected within 30 min of reaction, as displayed in figure 6(a). Therefore, we make sure that the quasi-spherical nanoparticles formed prior to the nanotriangles. Obviously, gold nanotriangles had not formed before 30 min of reaction. The longer wavelength absorbance settles at about 1000 nm after completion of reaction. Although the dried biomass fulfilled the reduction of chloroaurate ions, they failed to protect most of the quasi-spherical nanoparticles from aggregating because the water-soluble biomolecules that could specifically adsorb onto spherical nanoparticles to act as protecting agents were deficient. Since the nascent nanocrystals devoid of protection were unstable in the thermodynamic sense, the spherical nanoparticles shown in figures 7(a)–(c) that were produced early on might be stable owing to the shelter of the protecting biomolecules. By contrast, those formed later on might be less stable because such biomolecules were less available. Gold nanotriangles might grow by a process involving rapid reduction, assembly and room-temperature sintering of spherical gold nanoparticles [24]. The burst of smaller spherical nanoparticles prone to aggregation sped up their sintering into anisotropic particles with time, particularly in the later stage of the reaction. In other words, biomolecules as reductants have a significant advantage over their counterparts as protecting agents and weak passivation of surfaces of the nascent nanocrystals consequently promotes their chain amalgamation. It is evident that sintering of some nanoparticles and their adherence to the nanotriangle could be tracked as some particle-like protuberances were displayed on the surface of the nanotriangle in figure 7(e). The freshly shaped nanotriangles had high surface energy and it should suffer a shrinking process in order to reduce their surface energy to a minimum level. The process did not produce sharp-angled nanotriangles, but blunt-angled nanotriangles. When 0.5 g biomass was used to reduce the aqueous $HAuCl_4$,

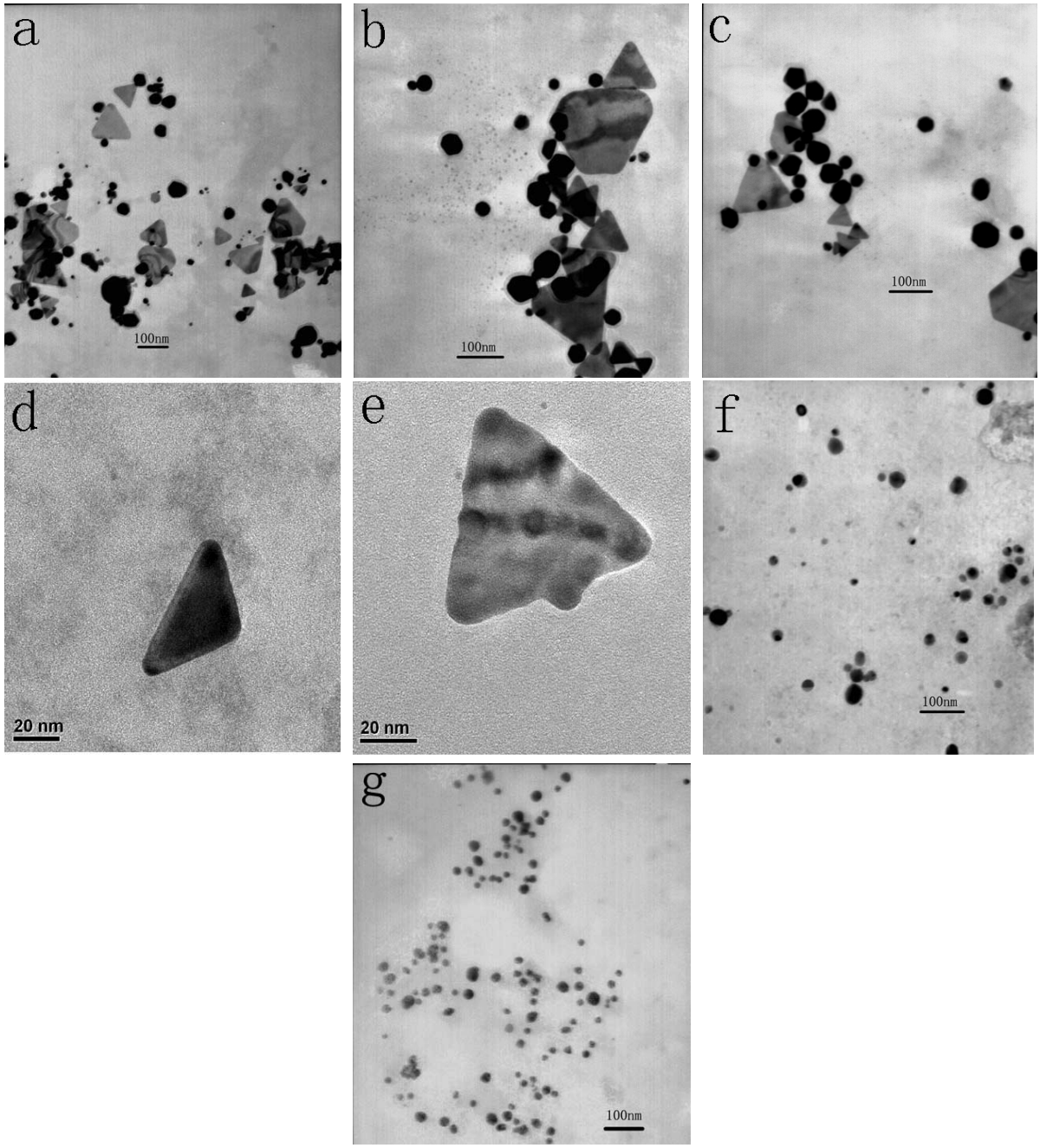

Figure 7. TEM images illustrating the formation of gold nanoparticles by exposing (a)–(e) 0.1 g, (f) 0.5 g, biomass to 50 ml, 1 mM aqueous $HAuCl_4$ at 30 °C. Scale bars: (a)–(c) 100 nm; (d) and (e)20 nm; (f) 200 nm; (g) 100 nm.

the biomolecules acting as capping agents strongly shaped spherical nanoparticles rather than nanotriangles though the reductive biomolecules were enhanced. The biomass offers sufficient protective biomolecules. Thus, strong interaction between such biomolecules and surfaces of the shaped nanoparticles prevent nascent gold nanocrystals from rapid sintering. When the biomass of 1.0 g dosage was employed, the interaction was intensified, leading to size reduction of the spherical nanoparticles in comparison with those by the 0.5 g biomass. Sastry *et al* elucidated that formation of gold nanotriangles by the Turkevich method using citrate reduction was highly favoured at low temperatures [34]. However, it was found herein that formation of gold nanotriangles by *C. camphora* leaf at ambient temperature strongly depended on the amount of the dried biomass.

3.3. Pronounced difference of shape control between gold and silver nanoparticles by C. camphora leaf

The pronounced difference of shape control between gold and silver nanoparticles has not been well elucidated. Sastry *et al* pondered that it could be due to the differences in weak binding of the biomolecules with the surface of silver nanoparticles [29]. Weaker binding of these biomolecules with

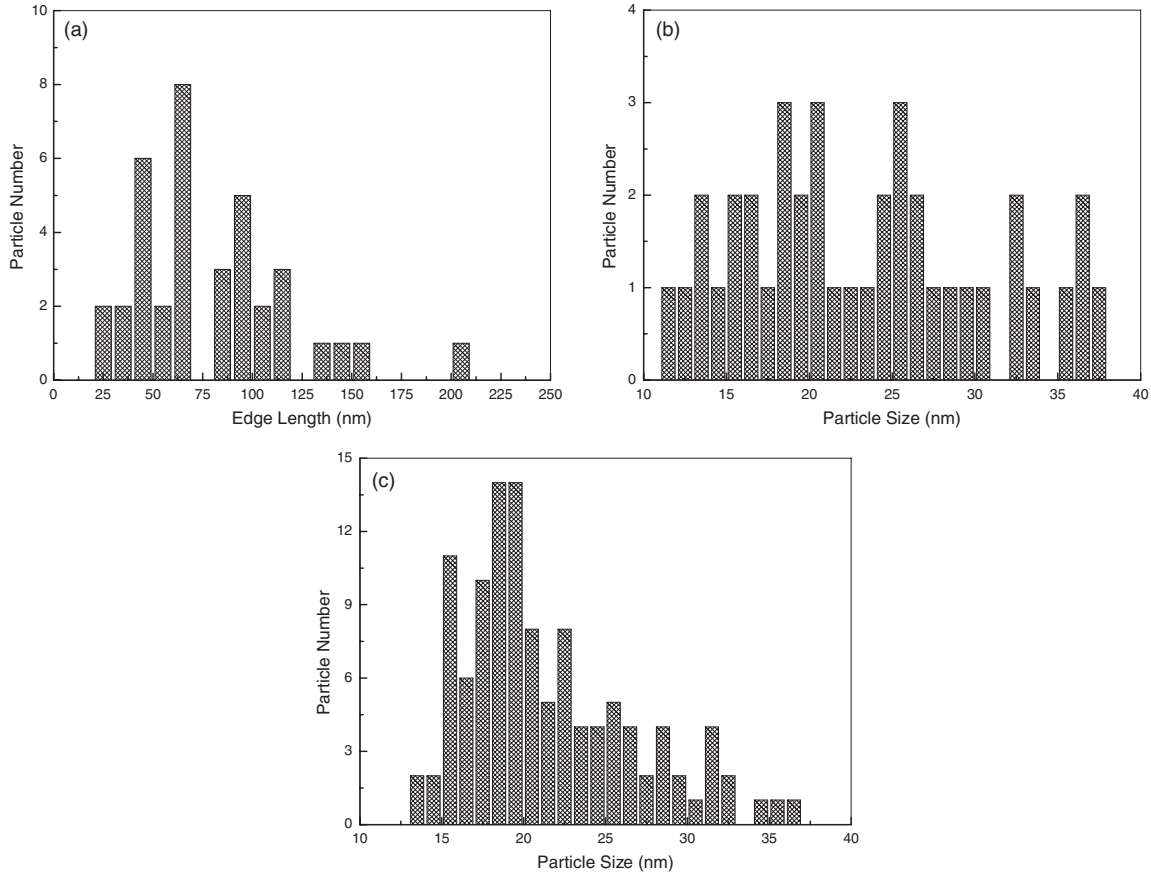

Figure 8. Size distribution of gold nanoparticles synthesized. (a) A histogram of edge length distribution of gold nanotriangles in figures 7(a)–(c). The average edge length is about 80.0 nm; (b) a histogram of size distribution of spherical gold nanoparticles by 0.5 g biomass in figure 7(f). The average particle size is about 23.4 nm; (c) a histogram of size distribution of spherical gold nanoparticles by 1.0 g biomass in figure 7(g). The average particle size is about 21.5 nm.

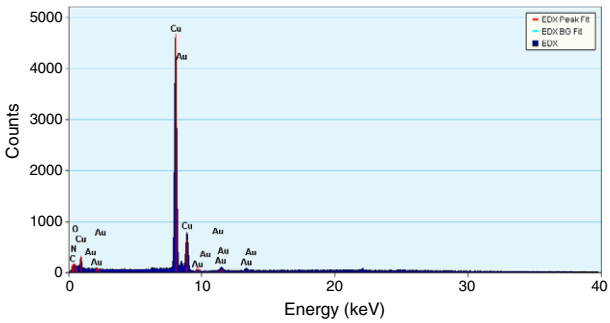

Figure 9. Energy dispersive x-ray spectrum of gold nanotriangles resulting from the before-mentioned experiment using 0.1 g biomass. The different x-ray emission peaks are labelled.

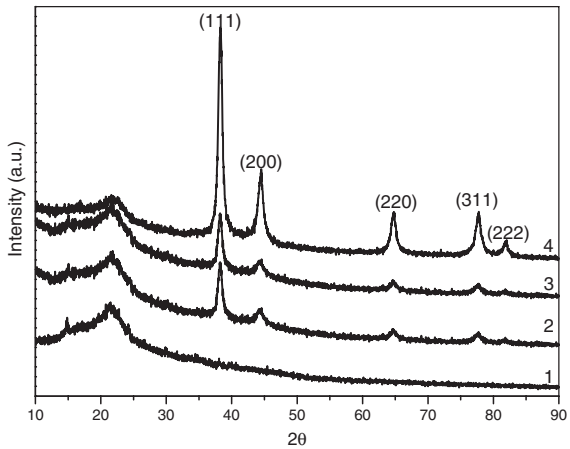

Figure 10. X-ray diffraction patterns of the as-prepared nanoparticles. Labelled peaks correspond to the characteristic diffraction peaks of elemental Au(0). Pattern 1 was obtained by XRD analysis of the sundried leaf. Patterns 2, 3 and 4 were derived from XRD analysis of the dried mixtures after reaction of 1.0, 0.5 and 0.1 g, biomass with 50 ml, 1 mM aqueous solution of $HAuCl_4$, respectively.

nascent silver nanocrystals could lead to isotropic growth of the crystals and thus formation of spherical particles [29]. As far as silver ions are concerned, the biomass offers affluent protective biomolecules but comparatively lean reductive counterparts when the synthetic recipes employing 0.1 or 0.5 g biomass were adopted. Nascent silver nanocrystals produced gradually were enclosed by the protective molecules. As a result, it eliminated rapid sintering of smaller nanoparticles, which is mainly responsible for the formation of the nanotriangles. It is notable that the protective biomolecules could not firmly resist the growth of anisotropic nanoparticles when 1.0 g biomass

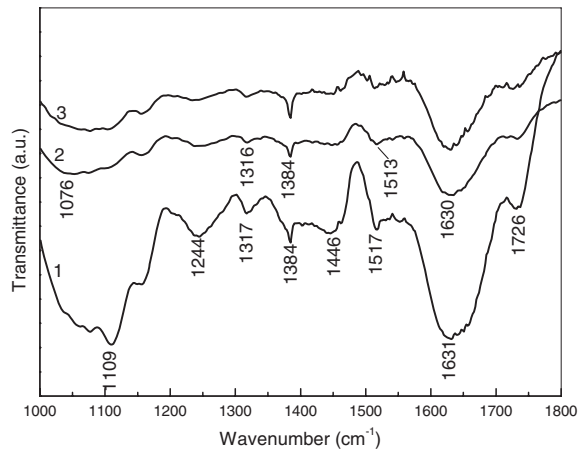

Figure 11. Typical FTIR absorption spectra of the leaf biomass before bioreduction (1), after bioreduction of silver ions (2) and after bioreduction of chloroaurate ions (3).

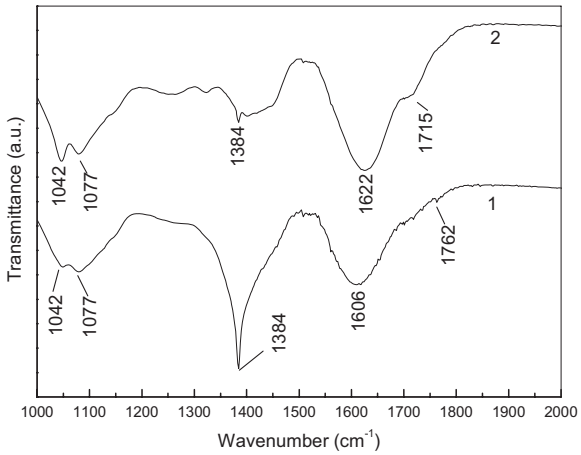

Figure 12. Typical FTIR absorption spectra of the dried silver nanoparticles (1) and gold nanoparticles (2).

was introduced into the same solution of silver nitrate. It would promote the effect of Ostwald ripening [35]. Remarkable augmentation of the reductive biomolecules makes some nascent crystals rapidly sinter into anisotropic nanostructures under rapid bioreduction. Some anisotropic particles of silver including a few quasi-nanotriangles could be produced, as seen in figure 2(c). Conversely, for chloroaurate ions, the reductive biomolecules dictated the formation of gold nanotriangles when the dosage of dried biomass was 0.1 g. When the dosage was increased to 0.5 or 1.0 g, it allowed the protective biomolecules to have control over the formation of the spherical nanoparticles. It would reduce the effect of Ostwald ripening [35] and pose a diffusion-controlled process. The diffusion current of gold atoms across the grain boundary would be curbed by the protective biomolecules. As reaction time elapses, the boundary of the produced particles expands in an isotropic fashion even though the reductive biomolecules augment enormously with the increase of biomass. Owing to the rich reductive biomolecules, however, the nuclei of gold species form simultaneously at the commencement of the bioreduction, with little subsequent nucleation of smaller particles [35]. As a consequence, the nucleation process is relatively fast while the growth process remains relatively slow [34], resulting in gold nanoparticles with narrow size distribution. In conclusion, the more the dosage of the biomass, the stronger the interaction between biomolecules and nascent nanocrystals. However, with the increase of biomass dosage, the interaction between the protective biomolecules and nascent gold nanocrystals was remarkably enhanced so that the addition of gold atoms to the surfaces of the nanocrystals was slowed down. In contrast, with the dosage increasing, the interaction between the protective biomolecules and nascent silver nanocrystals was little strengthened while the addition of silver atoms to surfaces of the nanocrystals was expedited. It allows rapidly produced silver atoms to get through the protective biomolecules and reach the surfaces of the nanocrystals in a drastic manner. In a word, the marked difference of shape control between gold and silver nanoparticles may be attributed to the comparative advantage of protective biomolecules and reductive biomolecules in the bioreduction of silver ions and chloroaurate ions by the biomass.

3.4. FTIR analysis results of the biomass before and after bioreduction

Our previous study on extraction of pharmaceutical components from the *C. camphora* leaf showed that alkaloids, flavones, hydroxybenzenes, anthracenes, steroids, terpenoids, coumarins, lactones, linalools, polysaccharides, amino acids and proteins exist in such a leaf [30, 36]. FTIR absorption spectra of the dried biomass of *C. camphora* leaf before and after bioreduction, as shown in figure 11, can offer information regarding the chemical change of the functional groups involved in bioreduction. Some absorbance bands centred at 1109, 1244, 1317, 1384, 1446, 1517, 1631 and 1726 cm^{-1} are observed in the region 1000–1800 cm^{-1}. Among them, the absorbance bands at 1109, 1631 and 1726 cm^{-1} in curve 1 were associated with the stretch vibration of –C–O, –C=C, RHC=O, respectively [37]. To a large extent, the band at 1109 cm^{-1} might be contributed by the –C–O groups of the polyols such as flavones, terpenoids and polysaccharides in the biomass. It could be figured out by comparison of curve 1, curve 2 and curve 3 that the disappearance of the band at 1109 cm^{-1} after bioreduction shows that the polyols are mainly responsible for the reduction of silver ions or chloroaurate ions. It is speculated that the alcohol groups are oxidized to carbonyl groups, thus leading to the band 1726 cm^{-1}. All in all, the water-soluble fractions in the biomass played complicated roles in the bioreduction of the precursors and shape evolution of the nanoparticles.

3.5. FTIR analysis results of silver and gold nanoparticles

Representative FTIR spectra of the obtained nanoparticles are shown in figure 12, which manifests several absorption peaks located at about 1042, 1077, 1384, 1606, 1622, 1715 and 1762 cm^{-1} in the region 1000–2000 cm^{-1}. The two absorption peaks located at around 1042 and 1077 cm^{-1} can be assigned as the absorption peaks of –C–O–C– or –C–O– [37]. Moreover, the wide absorption spectra at about 1606

and 1622 cm^{-1} may result from the stretching vibration of –C=C– [37]. In addition, there are some weak absorption spectra in the region 1700–1800 cm^{-1}, which can be attributed to the stretching vibration of –C=O [37]. For silver nanoparticles, the absorption at about 1384 cm^{-1} (curve 1) was notably enhanced in that NO_3^- existed in the residual solution [38]. To a large extent, the bonds or functional groups, such as –C–O–C–, –C–O–, –C=C– and –C=O, derive from the heterocyclic compounds that are water-soluble components in the dried biomass. Therefore, it is thought that the water-soluble heterocyclic compounds, e.g. alkaloids, flavones and anthracenes, are the capping ligands of the nanoparticles. In the polyol synthesis extensively studied for silver or gold nanoparticles, both oxygen and nitrogen atoms of the pyrrolidone unit can facilitate the adsorption of PVP onto the surface of metal nanostructures to fulfil the protection of the nanoparticles [39]. Likewise, the oxygen atoms herein might facilitate the adsorption of the heterocyclic components onto the particle surface in stabilizing the nanoparticles.

3.6. Sundried leaf versus leaf broth

Most of the previous research on synthesis of Ag or Au nanoparticles using plant extracts employed a broth resulting from boiling fresh plant leaves. We deem that the sundried biomass has some advantages over the broth. The approach using the broth suffers from two main drawbacks. Firstly, most of the leaves are seasonal so that fresh leaves would not be readily available for the bioreduction all the time. Secondly, it is fairly difficult to control some parameters accurately such as the optimum boiling time when the broth is attained. However, our work demonstrated that the route using the sundried biomass could circumvent these two limitations. On the one hand, the sundried biomass could be preserved as an excellent bioreductant, conveniently available any time for biosynthesis of the nanoparticles. On the other hand, not only could silver nanoparticles with concentrated size distribution be fabricated, but also triangular or spherical nanoparticles of gold could be facilely controlled by simply adjusting the amount of dried biomass. The bioreduction above proceeded extracelluarly so that few nanoparticles were bound by the biomass residue and almost all nanoparticles were dispersed in the suspension. The approach to silver and gold nanoparticles by *C. camphora* leaf has the same advantage as downstream processing and handling of the nanoparticle suspension would be much easier. It would be of practical value to develop a cost-effective biochemical process for mass-producing the nanoparticles by sundried *C. camphora* leaf. Beyond all doubt, the utilization of sundried *C. camphora* leaf for biosynthesis of the nanoparticles has defects. For example, the drying process of the leaf in the sun is time-consuming. Moreover, there is more biomass residue in the resulting hydrosols of nanoparticles using sundried leaf powder than fresh leaf broth.

4. Conclusions

In summary, we demonstrated a bioreductive approach to silver and gold nanoparticles using novel sundried biomass of *C. camphora* leaf. The size dispersity of quasi-spherical silver nanoparticles as well as triangular or spherical shapes of gold nanoparticles could be facilely controlled by simple variation of the amount of biomass reacting with aqueous solution of $AgNO_3$ or $HAuCl_4$. The marked difference of shape control between gold and silver nanoparticles may be attributed to the comparative advantage of protective biomolecules and reductive biomolecules. The polyol components and the water-soluble heterocyclic components were mainly responsible for the reduction of silver ions or chloroaurate ions and the stabilization of the nanoparticles, respectively. Instead of the boiled leaf broth from previous studies, sundried *C. camphora* leaf appears to be an environmentally friendly and low-cost candidate as reductant for synthesizing silver or gold nanoparticles.

Acknowledgments

This work is supported by the National Natural Science Foundation of China (Grant Nos 20576109 and 20376076). The authors thank the Analysis and Testing Centre of Xiamen University for the analysis and observation work, and Professor Zhaoxiong Xie, Dr Jianmei Li and Dr Haiming Zhang for their help in this study.

References

[1] Chan W C W and Nie S 1998 *Science* **281** 2016
[2] Tian Z and Ren B 2004 *Annu. Rev. Phys. Chem.* **55** 197
[3] Klefenz H 2004 *Eng. Life Sci.* **4** 211
[4] Debaditya B and Rajinder G 2005 *Crit. Rev. Biotechnol.* **25** 199
[5] Mandal D, Bolander M E, Mukhopadhyay D, Sarkar G and Mukherjee P 2006 *Appl. Microbiol. Biotechnol.* **69** 485
[6] Gardea-Torresdey J L, Tiemann K J, Gomez E, Dokken K, Tehuacanero S and Jose-Yacaman M 1999 *J. Nanopart. Res.* **1** 397
[7] Klaus T, Joerger R, Olsson E and Granqvist C 1999 *Proc. Natl Acad. Sci.* **96** 13611
[8] Fu J, Liu Y, Gu P, Tang D, Lin Z, Yao B and Wen S 2000 *Acta Phys.-Chim. Sin.* **16** 779
[9] Nair B and Pradeep T 2002 *Cryst. Growth Des.* **2** 293
[10] Yong P, Rowson N, Farr J P G, Harris I and Macaskie L 2002 *Biotechnol. Bioeng.* **80** 369
[11] Zhang H, Li Q, Lu Y, Sun D, Lin X, Deng X, He N and Zheng S 2005 *J. Chem. Technol. Biotechnol.* **80** 285
[12] Fu M, Li Q, Sun D, Lu Y, He N, Deng X, Wang H and Huang J 2006 *Chin. J. Chem. Eng.* **14** 114
[13] Mukherjee P *et al* 2001 *Angew. Chem. Int. Edn* **40** 3585
[14] Mukherjee P *et al* 2001 *Nano Lett.* **1** 515
[15] Mukherjee P, Senapati S, Mandal D, Ahmad A, Khan M I, Kumar R and Sastry M 2002 *ChemBioChem* **3** 461
[16] Sastry M, Ahmad A, Khan M I and Kumar R 2003 *Curr. Sci.* **85** 162
[17] Ahmad A, Mukherjee P, Senapati S, Mandal D, Khan M I, Kumar R and Sastry M 2003 *Colloids Surf.* B **28** 313
[18] Ahmad A, Senapati S, Khan M I, Kumar R and Sastry M 2005 *J. Biomed. Nanotechnol.* **1** 47
[19] Gardea-Torresdey J L, Parsons J G, Dokken K, Peralta-Videa J, Troiani H E, Santiago P and Jose-Yacaman M 2002 *Nano Lett.* **2** 397
[20] Gardea-Torresdey J L, Gomez E, Peralta-Videa J, Parsons J G, Troiani H and Jose-Yacaman M 2003 *Langmuir* **19** 1357
[21] Shankar S S, Ahmad A, Pasricha R and Sastry M 2003 *J. Mater. Chem.* **13** 1822
[22] Shankar S S, Ahmad A and Sastry M 2003 *Biotechnol. Prog.* **19** 1627

[23] Shankar S S, Rai A, Ahmad A and Sastry M 2004 *J. Colloid Interface Sci.* **275** 496
[24] Shankar S S, Rai A, Ankamwar B, Singh A, Ahmad A and Sastry M 2004 *Nat. Mater.* **3** 482
[25] Ankamwar B, Damle C, Ahmad A and Sastry M 2005 *J. Nanosci. Nanotechnol.* **5** 1665
[26] Ankamwar B, Chaudhary M and Sastry M 2005 *Synth. React. Inorg. Met.-Org. Nano-Metal Chem.* **35** 19
[27] Shankar S S, Rai A, Ahmad A and Sastry M 2005 *Chem. Mater.* **17** 566
[28] Rai A, Singh A, Ahmad A and Sastry M 2006 *Langmuir* **22** 736
[29] Chandran S P, Chaudhary M, Pasricha R, Ahmad A and Sastry M 2006 *Biotechnol. Prog.* **22** 577
[30] Su Y, Li Q, Yao C, Lu Y and Hong J 2006 *Chin. Chem. Ind. Eng. Prog.* **25** 200
[31] Wiley B J, Im S H, McLellan J, Siekkinen A and Xia Y 2006 *J. Phys. Chem.* B **110** 15666
[32] Burda C, Chen X, Narayanan R and El-Sayed M A 2005 *Chem. Rev.* **105** 1025
[33] Daniel M and Astruc D 2004 *Chem. Rev.* **104** 293
[34] Shankar S S, Bhargava S and Sastry M 2005 *J. Nanosci. Nanotechnol.* **5** 1721
[35] Cushing B L, Kolesnichenko V L and O'Connor C J 2004 *Chem. Rev.* **104** 3893
[36] Gao J 2003 *Botanic Chemistry* (Beijing: Scientific Publisher)
[37] Zhu M 2000 *Apparatus Analyses* (Beijing: Higher Education Press)
[38] Luo L, Yu S, Qian S and Zhou T 2005 *J. Am. Chem. Soc.* **127** 2822
[39] Xiong Y, Washio I, Chen J, Cai H, Li Z and Xia Y 2006 *Langmuir* **22** 8563